

Real-Time Out-of-Equilibrium Quantum Dynamics in Disordered Materials

Luis M. Canonico,^{1,*} Stephan Roche,^{1,2} and Aron W. Cummings^{1,†}

¹*Catalan Institute of Nanoscience and Nanotechnology (ICN2),
CSIC and BIST, Campus UAB, Bellaterra, 08193 Barcelona, Spain*

²*ICREA, Institució Catalana de Recerca i Estudis Avançats, 08070 Barcelona, Spain*
(Dated: July 24, 2024)

We report a linear-scaling numerical method for exploring nonequilibrium electron dynamics in systems of arbitrary complexity. Based on the Chebyshev expansion of the time evolution of the single-particle density matrix, the method gives access to nonperturbative excitation and relaxation phenomena in models of disordered materials with sizes on the experimental scale. After validating the method by applying it to saturable optical absorption in clean graphene, we uncover that disorder can enhance absorption in graphene and that the interplay between light, anisotropy, and disorder in nanoporous graphene might be appealing for sensing applications. Beyond the optical properties of graphene-like materials, the method can be applied to a wide range of large-area materials and systems with arbitrary descriptions of defects and disorder.

Understanding nonequilibrium charge dynamics is crucial for assessing electronic, energy, and angular momentum transport in quantum materials [1]. For instance, charge carriers propagating in graphene under optical excitation are quickly driven to a highly nonequilibrium state [2–10], and these “hot carriers” serve as the functioning principle for ultra-compact sensing and communication devices [11–13]. Examples of such devices are sensitive THz antennas [14], and saturable absorbers usable in mode-locked lasers [15–17]. Moreover, recent developments allow for the bottom-up growth of atomically-precise nanomaterials such as nanoporous graphene (NPG) [18], an array of covalently-linked graphene nanoribbons that exhibits a sizable band gap [18, 19] and strong in-plane transport anisotropy [19–22]. Such bottom-up engineering can thus imbue 2D carbon materials with properties appealing for sensing applications present in other 2D materials such as transition metal dichalcogenides [23] or black phosphorus [24].

The study of out-of-equilibrium processes requires a nonperturbative description of the carrier dynamics, for both the excitation of the system and the treatment of disorder. Disorder is a fundamental part of device fabrication and can drastically alter the energy transfer dynamics and optical response of any material, including graphene [25–27] and NPG [22]. Semiclassical [2, 8, 28] and microscopic [29–32] methods have been developed to study nonequilibrium processes, but despite their success, these techniques are not currently suited to deal with a nonperturbative description of disorder on typical experimental length scales. Meanwhile, real-space linear-scaling methods can study electron transport in systems containing many millions of atoms, reaching experimental scales, while treating disorder nonperturbatively [33, 34]. However, these methods have been restricted to first- and second-order expansions of the excitation process. Thus, the theoretical investigation of nonequilibrium phenomena in realistic systems calls for approaches that incorporate the best of both worlds.

In this Letter, we present a numerical method for simulating out-of-equilibrium electron dynamics in systems comprised of millions of atoms while treating disorder nonperturbatively. To illustrate the method’s capabilities, we use it to study saturable absorption in graphene and NPG in the presence of electrostatic disorder. We demonstrate that it can describe optical absorption nonperturbatively by tracking the time- and energy-resolved carrier distribution. Our results show excellent agreement with previous experiments in clean graphene, and indicate that electrostatic disorder may improve the performance of graphene saturable absorbers. We also demonstrate that NPG exhibits optical anisotropy that can be enhanced by weak disorder. While we have focused on optical absorption, this method is completely generalizable, making it suitable for studying far-from-equilibrium electron dynamics in various materials and systems approaching experimental length scales while considering nonperturbative disorder effects.

Methodology – The core aspect of the methodology is the time evolution of the density matrix. To explore nonequilibrium dynamics, we want to track its evolution under a time-varying Hamiltonian. We start with the ground state density matrix, represented by the Fermi operator $\hat{F}(\hat{H}_0, T_0, \mu_0) = [1 + \exp((\hat{H}_0 - \mu_0)/k_B T_0)]^{-1}$, where \hat{H}_0 is the Hamiltonian in equilibrium while T_0 and μ_0 are the initial electronic temperature and chemical potential [35–38]. Under a Hamiltonian that evolves from its equilibrium state $\hat{H}_0 \rightarrow \hat{H}(t)$, we then calculate the time-dependent electron occupation as

$$\langle n(\varepsilon, t) \rangle = \frac{\text{Tr}\{\hat{U}^\dagger(t, 0)\delta(\hat{H}(t) - \varepsilon)\hat{U}(t, 0)\hat{F}(\hat{H}_0, T_0, \mu_0)\}}{\text{Tr}\{\delta(\hat{H}(t) - \varepsilon)\}}, \quad (1)$$

where $\hat{U}(t_1, t_0) = \hat{\mathcal{T}} \exp\left\{-\frac{i}{\hbar} \int_{t_0}^{t_1} \hat{H}(t') dt'\right\}$ is the time-ordered evolution operator and $\delta(\dots)$ is the Dirac delta operator, which projects the occupation onto energy ε .

We approximate the trace as an average over random phase states [33, 39], $\text{Tr}\{\hat{A}\} \approx \frac{1}{R} \sum_{r=0}^R \langle \psi_r | \hat{A} | \psi_r \rangle$, where

in the site basis $|\psi_r\rangle = \frac{1}{\sqrt{N}} [e^{i\xi_1} \dots e^{i\xi_N}]^T$, ξ_n is a random number evenly distributed in $[0, 2\pi)$ and N is the number of sites. In general, for a good approximation one only needs a few states, $R \ll N$ [33, 39].

In Eq. (1) we have to determine the time evolution of the vectors $|\psi_r(t)\rangle \equiv \hat{U}(t, 0)|\psi_r\rangle$ and $|\psi_r^{\hat{F}}(t)\rangle \equiv \hat{U}(t, 0)\hat{F}(\hat{H}_0, T_0, \mu_0)|\psi_r\rangle$. For short simulation time steps Δt , $|\psi_r(t)\rangle$ can be evolved using the instantaneous Hamiltonian, such that $|\psi_r(t + \Delta t)\rangle = \hat{U}(t + \Delta t, t)|\psi_r(t)\rangle \approx \exp(-i\hat{H}(t)\Delta t/\hbar)|\psi_r(t)\rangle$. In contrast, $|\psi_r^{\hat{F}}(t)\rangle$ contains the full history of the electron occupation. In addition to the accumulation of energy driven by $\hat{H}(t)$, we would like to track other processes, not necessarily captured by $\hat{H}(t)$, that modify the electron occupation. For example, high-energy electrons may emit phonons, dumping energy to the lattice and relaxing to a thermal distribution at the lattice temperature [8, 25, 40]. Meanwhile, carrier-carrier scattering in graphene conserves the total energy of the electrons but drives them toward a thermal distribution that may be much higher than the lattice temperature [2, 10, 41].

To that end, we propose a modified time evolution for $|\psi_r^{\hat{F}}(t)\rangle$ that captures both a time-varying Hamiltonian and relaxation toward a given carrier distribution,

$$\frac{\partial}{\partial t} |\psi_r^{\hat{F}}(t)\rangle = -\frac{i}{\hbar} \hat{H}(t) |\psi_r^{\hat{F}}(t)\rangle - \frac{1}{\tau} \left(|\psi_r^{\hat{F}}(t)\rangle - \hat{N}_{\text{eq}}(t) |\psi_r(t)\rangle \right), \quad (2)$$

where $\hat{N}_{\text{eq}}(t)$ is the instantaneous equilibrium distribution toward which the electrons relax, over a time scale τ . As stated above, this could be driven by electron-phonon or electron-electron scattering, or could be any other distribution governed by the physics of the system.

In general, $\hat{N}_{\text{eq}}(t)$ can vary in time and may depend on the instantaneous carrier distribution, as in the case of electron-electron scattering. Additionally, complex terms in the Schrödinger equation lead to vanishing carrier density [42]. We thus perform the time evolution of Eq. (2) in two steps. First we compute $|\psi_r(t + \Delta t)\rangle = \hat{U}(t + \Delta t, t)|\psi_r(t)\rangle$ and $|\psi_r^{\hat{F}}(t + \Delta t)\rangle = \hat{U}(t + \Delta t, t)|\psi_r^{\hat{F}}(t)\rangle$. Next, from these updated vectors we determine a new carrier distribution $\hat{N}_{\text{eq}}(t + \Delta t)$ and mix it with $|\psi_r^{\hat{F}}(t + \Delta t)\rangle$ using forward time stepping. Equation (2) then becomes

$$|\psi_r^{\hat{F}}(t + \Delta t)\rangle \approx \left(1 - \frac{\Delta t}{\tau} \right) \hat{U}(t + \Delta t, t) |\psi_r^{\hat{F}}(t)\rangle + \frac{\Delta t}{\tau} \hat{N}_{\text{eq}}(t + \Delta t) \hat{U}(t + \Delta t, t) |\psi_r(t)\rangle. \quad (3)$$

In the application to graphene below, we assume \hat{N}_{eq} is given by electron-electron scattering, which drives $\langle n(\varepsilon, t) \rangle$ toward a thermal distribution over a time scale τ_{ee} . Thus, $\hat{N}_{\text{eq}}(t) = \hat{F}(\hat{H}(t), T(t), \mu(t))$, where at each

time step we determine the temperature $T(t)$ and the chemical potential $\mu(t)$ to ensure the conservation of energy and carrier density [43].

Equations (1) and (3) require evaluation of the functions $\delta(\hat{H}(t) - \varepsilon)$ and $\exp(-i\hat{H}(t)\Delta t/\hbar)$. We efficiently evaluate these by expanding them as a series of Chebyshev polynomials [33, 39, 44, 45], and the method thus boils down to a series of multiplies between the matrix $\hat{H}(t)$ and the vectors $|\psi_r(t)\rangle$ and $|\psi_r^{\hat{F}}(t)\rangle$ (see SM for details about the Chebyshev expansion [43]). For sparse tight-binding Hamiltonians, the total simulation cost is then $\mathcal{O}(RMN_tN)$, where M is the number of Chebyshev polynomials and N_t is the number of time steps. R , M , and N_t are decoupled from N , and the method thus scales linearly with the number of sites [33], allowing for the calculation of time-resolved nonequilibrium dynamics in systems reaching the experimental scale. Below, we simulate samples with $512 \times 512 \times 4$ and $64 \times 128 \times 80$ carbon atoms for graphene and NPG, respectively.

Optical excitations in graphene – To demonstrate the methodology, we examine the evolution of the carrier distribution in graphene when illuminated by a linearly-polarized optical pulse. We consider a minimal tight-binding model of graphene [46], $\hat{H} = -\sum_{\langle i,j \rangle} t_{ij} c_i^\dagger c_j + \sum_i V_i c_i^\dagger c_i$, where the first term is the nearest-neighbor hopping, with $t_{ij} = t = 2.71$ eV. The second term represents electrostatic disorder. Here we use Anderson disorder, where V_i is a random onsite potential evenly distributed in $[-W/2, W/2]$ with W the disorder strength.

To include the linearly-polarized optical field, we define a vector potential $\mathbf{A}(t) = A_0 P(t) \sin(\omega_p t) \hat{y}$, where A_0 is the amplitude, $P(t)$ is the envelope of the optical pulse, and $\hbar\omega_p$ is the photon energy [47]. Using the Peierls substitution, the nearest-neighbor hopping becomes

$$t_{ij}(t) = t \exp \left(i \frac{2\pi}{\Phi_0} \int_{\mathbf{r}_i}^{\mathbf{r}_j} d\mathbf{r} \cdot [A_0 P(t) \sin(\omega t) \hat{y}] \right), \quad (4)$$

where \mathbf{r}_i is the position of carbon site i and $\Phi_0 = h/e$ is the magnetic flux quantum. Below we set $A_0 = \Gamma \Phi_0 / 2a$, where Γ is a free parameter to regulate the field intensity and $a = 2.46$ Å is the graphene lattice constant.

To validate the methodology, we first consider clean graphene without relaxation, $W = 0$ and $\tau \rightarrow \infty$. We apply an optical pulse with an envelope $P(t) = \text{sech}[(t - 2T_p)/\gamma T_p]$, where $T_p = 2\pi/\omega_p$ is the period of field oscillation and $\gamma \approx 0.5673$, such that the full width of $P^2(t)$ at half maximum is equal to T_p [48]. We consider a simulation time of $t = 0 \rightarrow 4T_p$.

Figures 1(a) and (b) show the time evolution of an initially undoped carrier distribution at zero temperature, when illuminated by pulses with $\hbar\omega_p = 0.8$ eV and 0.6 eV, respectively. In both cases the field amplitude was set to $\Gamma = 2.5 \times 10^{-2}$. Absorption peaks develop at $\pm \hbar\omega_p/2$, as predicted by theory [28], with their width attributed to the finite pulse duration and the numerical broaden-

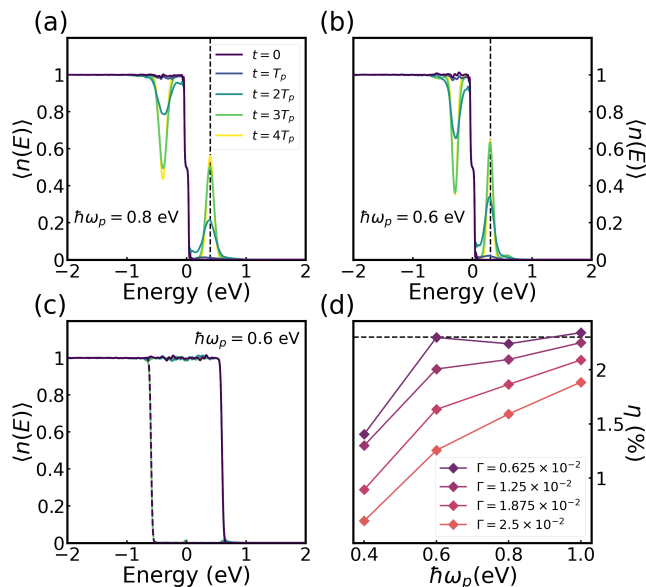


FIG. 1. Time evolution of the graphene carrier occupation for photon energies (a) $\hbar\omega_p = 0.8$ eV and (b) 0.6 eV, with $\mu_0 = 0$. The dashed lines indicate the expected absorption peak at $\hbar\omega_p/2$. (c) Evolution of n - and p -doped distributions with $\mu_0 = \pm 0.6$ eV (solid and dashed lines, respectively), indicating Pauli blocking. (d) Absorption efficiency vs. photon energy for different optical intensities. In all cases, $T_0 = 0$ K with a pulse envelope $P(t) = \text{sech}[(t - 2T_p)/\gamma T_p]$, where $T_p = 2\pi/\omega_p$ and $\gamma \approx 0.5673$.

ing inherent in the Chebyshev expansion of $\delta(\hat{H}(t) - \varepsilon)$ [33, 39]. It is also worth noting that the height of the absorption peak increases with decreasing photon energy; because of its longer duration, the total energy delivered by the 0.6-eV pulse is greater than for 0.8 eV.

Figure 1(c) confirms that the method obeys the Pauli exclusion principle. Here we show the evolution of n - and p -doped carrier distributions, with $\mu_0 = \pm 0.6$ eV, under an optical pulse with $\hbar\omega_p = 0.6$ eV. This figure shows that for $|\mu_0| > \hbar\omega_p/2$, Pauli blocking forbids any carrier excitation from the valence to the conduction band.

Finally, we show that the method recovers the universal optical absorption of graphene [3, 4]. To quantify this, we calculate the energy absorption efficiency,

$$\eta(t) = \frac{E_{\text{el}}(t) - E_{\text{el}}(0)}{E_{\text{opt}}(t)}, \quad (5)$$

where $E_{\text{el}}(t) = \langle \psi_r(t) | \hat{H}(t) | \psi_r^{\hat{F}}(t) \rangle$ is the energy of the electrons and $E_{\text{opt}}(t) = A_S \epsilon_0 c \int_0^t |\partial_t \mathbf{A}(t)|^2 dt$ is the total energy irradiated over the sample at time t , where A_S , ϵ_0 and c are the sample area, vacuum permittivity, and speed of light, respectively [49]. In Fig. 1(d) we plot $\eta(t = 4T_p)$ as a function of $\hbar\omega_p$ for different optical intensities Γ . In the limit of low total optical energy (smaller Γ and higher $\hbar\omega_p$), the absorption efficiency reaches the predicted universal value of $\sim 2.3\%$, indicated by the hor-

izontal dashed line. Meanwhile, at higher optical energy the efficiency decreases due to the onset of saturable absorption arising from Pauli blocking.

Saturable absorption in graphene – Having verified the basic features of optical absorption, we now use the method to compare to measurements of saturable absorption in graphene [17]. To mimic the experimental conditions we let $\mu_0 = -5$ meV and $T_0 = 300$ K, we apply a 63-fs optical pulse with energy $\hbar\omega_p = 1.55$ eV, and we add an absorption background of 0.4% to our results. We also include electron-electron scattering with thermalization time τ_{ee} , see Eqs. (2) and (3).

In Fig. 2(a) we plot the energy absorption efficiency as a function of optical intensity. The black symbols are the experimental results [17], and the colored lines are our simulations. Each line corresponds to a different value of τ_{ee} . In agreement with the measurements, higher optical intensity leads to a reduction of absorption efficiency, owing to optical bleaching. Meanwhile, reducing τ_{ee} improves absorption efficiency at higher optical intensity, as faster thermalization redistributes the absorption peaks and suppresses Pauli blocking [50]. We find the best agreement between our simulations and the experiments when $\tau_{ee} = 25$ fs, which falls within the estimates for carrier-carrier relaxation times in graphene [41].

Figure 2(b) shows the evolution of the carrier distribution at high optical intensity for $\tau_{ee} = 25$ fs. There is a sizable buildup of carriers at $\pm \hbar\omega/2$, resulting in Pauli blocking and a reduction of the absorption efficiency. One can also see the impact of a short τ_{ee} , with the formation of a thermal distribution for $|\varepsilon| < \hbar\omega_p/2$. However, even with this short τ_{ee} , at high intensities carrier-carrier scattering cannot fully relax the absorption peaks, resulting in bleaching and poor absorber performance.

Next, we consider the same situation in the presence of real-space disorder. Figure 2(c) shows the absorption efficiency as a function of light intensity for various Anderson disorder strengths. Remarkably, absorption efficiency is enhanced with increasing disorder strength. This result correlates with the broadening of the density of states, which renormalizes the Fermi velocity and increases the number of states available for carrier excitation [43]. Meanwhile, even though absorption increases with disorder, we still see bleaching and a reduction of absorption with increasing optical intensity.

Figure 2(d) shows the evolution of the carrier distribution at high optical intensity, for $W = 3$ eV and $\tau_{ee} = 25$ fs. Compared to panel (b), one can see that the carrier dynamics of the disordered system drastically differ from the clean one. Specifically, disorder leads to a much more effective thermalization of carriers, as the broadening opens optical absorption pathways other than $-\hbar\omega_p/2 \rightarrow +\hbar\omega_p/2$ [2]. This enables enhanced absorption at low optical intensities while also suppressing bleaching at high intensities, and is similar to a ‘‘pre-thermalization’’ effect examined in Ref. 51.

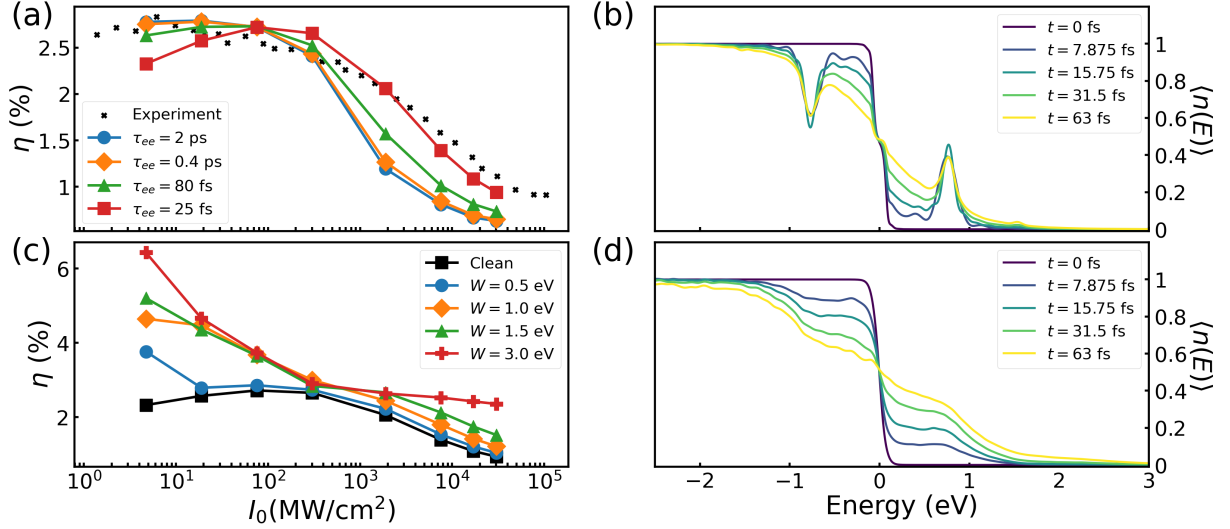


FIG. 2. (a) Energy absorption efficiency vs. light intensity for clean graphene with $\mu_0 = -5$ meV and $T_0 = 300$ K, under a 63-fs optical pulse with $\hbar\omega_p = 1.55$ eV. Black symbols are experimental data [17], and colored lines are simulations with varying τ_{ee} . (b) Time-dependent carrier distribution at high intensity ($I_0 = 3.02 \times 10^4$ MW/cm 2) for $\tau_{ee} = 25$ fs. (c) Energy absorption efficiency vs. light intensity in the presence of Anderson disorder, for the same conditions as in panel (a), with $\tau_{ee} = 25$ fs. (d) Time-dependent carrier distribution at high intensity ($I_0 = 3.02 \times 10^4$ MW/cm 2) for Anderson disorder strength $W = 3$ eV.

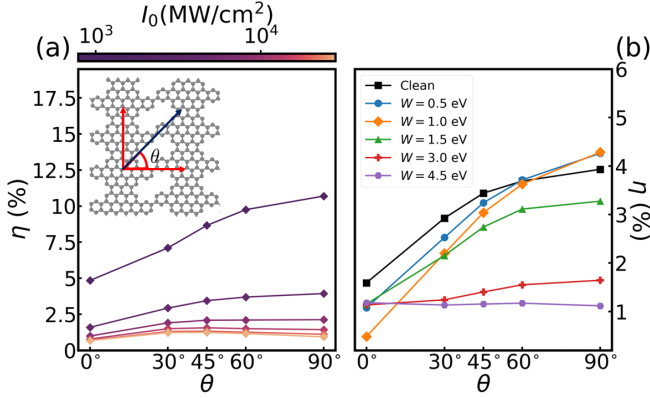


FIG. 3. (a) Anisotropic energy absorption of NPG for $\mu_0 = -0.1$ eV, $T_0 = 300$ K and $\tau_{ee} = 25$ fs under a 97.65-fs pulse with $\hbar\omega_p = 1$ eV at various optical intensities. Inset: Schematic of NPG used in our simulations. The red arrows are the ribbon axes and the blue arrow is the direction of light polarization. (b) Angle-dependent energy absorption for disordered NPG under the same conditions, for $I_0 = 3.142 \times 10^3$ MW/cm 2 and various Anderson disorder strengths W .

Anisotropic absorption in nanoporous graphene – We now apply the method to NPG, to examine the impact of saturable absorption and disorder on its optical anisotropy. The inset of Figure 3(a) shows the structure of NPG. We model its electronic properties with the graphene Hamiltonian, which has been shown to reproduce the band structure obtained from DFT [19, 20, 22]. To analyze optical anisotropy, we define a vector potential $\mathbf{A}(t) = A_0 \sin(\omega t) [\cos(\theta)\hat{x} + \sin(\theta)\hat{y}]$, where θ is the

direction of light polarization, see Fig. 3(a). In our simulations, we let $\mu_0 = -0.1$ eV, $T_0 = 300$ K, $\tau_{ee} = 25$ fs, and we apply a 97.65-fs pulse with energy $\hbar\omega_p = 1$ eV.

Figure 3(a) shows the angle-dependent absorption in clean NPG at different optical intensities. Anisotropy is clearly visible at low intensity, with the ratio $\eta(90^\circ)/\eta(0^\circ) \approx 2.2$. Meanwhile, $\eta(0^\circ) > 0$ in all cases, consistent with a small but finite charge transport perpendicular to the ribbons [19, 20, 22]. On the other hand, increasing the light intensity triggers optical bleaching and suppresses the anisotropy, down to a ratio of ~ 1.4 at the highest intensity. Interestingly, at this intensity, we find that energy absorption is maximized at $\theta \approx 45^\circ$.

To analyze the impact of disorder, we fix the light intensity to $I_0 = 3.142 \times 10^3$ MW/cm 2 and calculate the angle-dependent absorption for various Anderson strengths. As seen in Fig. 3(c), weak disorder significantly enhances optical anisotropy, up to a ratio of ~ 9 for $W = 1$ eV. Most of this enhancement comes from a strong suppression of absorption perpendicular to the ribbons. This correlates with the rapid onset of electron localization in this direction, previously observed in quantum transport simulations [22].

In contrast, weak disorder enhances optical absorption parallel to the ribbons, similar to graphene. However, for $W \geq 1.5$ eV, both absorption and anisotropy are then suppressed, indicating the onset of electron localization. For highly disordered NPG ($W = 4.5$ eV), absorption is reduced to $\sim 1\%$ and becomes fully isotropic, indicating a subtle interplay between disorder and optical anisotropy that may be exploitable for sensing applications.

Summary and conclusions – We have presented a linear-scaling numerical method that enables the study of nonequilibrium carrier dynamics in systems with sizes reaching the experimental scale, with nonperturbative descriptions of defects and disorder. The methodology has been validated by capturing both universal absorption and saturable absorption in graphene, and it has then been used to predict disorder-induced enhancement of energy absorption and optical anisotropy in graphene and NPG. Beyond the optical properties of carbon-based 2D materials, this numerical methodology is generalizable to any time-dependent tight-binding Hamiltonian, which makes it applicable to the study of far-from-equilibrium electron dynamics in a large class of materials under a wide range of excitations.

L.M.C. acknowledges funding from the Ministerio de Ciencia e Innovación de España under grant no. PID2019-106684GB-I00 / AEI / 10.13039/501100011033, FJC2021-047300-I, financed by MCIN / AEI / 10.13039/501100011033 and the European Union “NextGenerationEU/PRTR”. L.M.C. and A.W.C. acknowledge funding from the U.S. Army Research Office under grant no. W911NF-21-1-0004. We acknowledge funding from Ministerio de Ciencia e Innovación under grant no. PID2019-106684GB-I00 financed by MCIN / AEI / 10.13039/501100011033. ICN2 is funded by the CERCA Programme/Generalitat de Catalunya and supported by the Severo Ochoa Centres of Excellence programme, Grant CEX2021-001214-S, funded by MCIN / AEI / 10.13039.501100011033.

* luis.canonico@icn2.cat

† aron.cummings@icn2.cat

- [1] A. C. Ferrari, F. Bonaccorso, V. Fal’ko, K. S. Novoselov, S. Roche, P. Bøggild, S. Borini, F. H. L. Koppens, V. Palermo, N. Pugno, *et al.*, [Nanoscale](#) **7**, 4598 (2015).
- [2] J. C. Song and L. S. Levitov, [J. Phys. Condens. Matter](#) **27**, 164201 (2015).
- [3] R. R. Nair, P. Blake, A. N. Grigorenko, K. S. Novoselov, T. J. Booth, T. Stauber, N. M. R. Peres, and A. K. Geim, [Science](#) **320**, 1308 (2008).
- [4] K. F. Mak, M. Y. Sfeir, Y. Wu, C. H. Lui, J. A. Misewich, and T. F. Heinz, [Phys. Rev. Lett.](#) **101**, 196405 (2008).
- [5] A. B. Kuzmenko, E. van Heumen, F. Carbone, and D. van der Marel, [Phys. Rev. Lett.](#) **100**, 117401 (2008).
- [6] J. M. Dawlaty, S. Shivaraman, J. Strait, P. George, M. Chandrashekhara, F. Rana, M. G. Spencer, D. Veksler, and Y. Chen, [Appl. Phys. Lett.](#) **93**, 131905 (2008).
- [7] K. J. Tielrooij, J. C. W. Song, S. A. Jensen, A. Centeno, A. Pesquera, A. Zurutuza Elorza, M. Bonn, L. S. Levitov, and F. H. L. Koppens, [Nat. Phys.](#) **9**, 248 (2013).
- [8] R. Bistritzer and A. H. MacDonald, [Phys. Rev. Lett.](#) **102**, 206410 (2009).
- [9] W.-K. Tse and S. Das Sarma, [Phys. Rev. B](#) **79**, 235406 (2009).
- [10] M. Massicotte, G. Soavi, A. Principi, and K.-J. Tielrooij, [Nanoscale](#) **13**, 8376 (2021).
- [11] F. Bonaccorso, Z. Sun, T. Hasan, and A. C. Ferrari, [Nat. Photonics](#) **4**, 611 (2010).
- [12] M. Romagnoli, V. Sorianello, M. Midrio, F. H. Koppens, C. Huyghebaert, D. Neumaier, P. Galli, W. Templ, A. D’Errico, and A. C. Ferrari, [Nat. Rev. Mater.](#) **3**, 392 (2018).
- [13] A. Antidormi and A. W. Cummings, [Phys. Rev. Appl.](#) **15**, 054049 (2021).
- [14] S. Castilla, B. Terrés, M. Autore, L. Viti, J. Li, A. Y. Nikitin, I. Vangelidis, K. Watanabe, T. Taniguchi, E. Lidorikis, M. S. Vitiello, R. Hillenbrand, K.-J. Tielrooij, and F. H. Koppens, [Nano Lett.](#) **19**, 2765 (2019).
- [15] Q. Bao, H. Zhang, Y. Wang, Z. Ni, Y. Yan, Z. X. Shen, K. P. Loh, and D. Y. Tang, [Adv. Funct. Mater.](#) **19**, 3077 (2009).
- [16] Q. Bao, H. Zhang, Z. Ni, Y. Wang, L. Polavarapu, Z. Shen, Q. Xu, D. Tang, and K. P. Loh, [Nano Res.](#) **4**, 297 (2010).
- [17] I. H. Baek, H. W. Lee, S. Bae, B. H. Hong, Y. H. Ahn, D.-I. Yeom, and F. Rotermund, [Appl. Phys. Express](#) **5**, 032701 (2012).
- [18] C. Moreno, M. Vilas-Varela, B. Kretz, A. Garcia-Lekue, M. V. Costache, M. Paradin, M. Panighel, G. Ceballos, S. O. Valenzuela, D. Peña, *et al.*, [Science](#) **360**, 199 (2018).
- [19] G. Calogero, N. R. Papior, B. Kretz, A. Garcia-Lekue, T. Frederiksen, and M. Brandbyge, [Nano Lett.](#) **19**, 576 (2018).
- [20] G. Calogero, I. Alcón, N. Papior, A.-P. Jauho, and M. Brandbyge, [J. Am. Chem. Soc.](#) **141**, 13081 (2019).
- [21] B. Mortazavi, M. E. Madjet, M. Shahrokhi, S. Ahzi, X. Zhuang, and T. Rabczuk, [Carbon](#) **147**, 377 (2019).
- [22] I. Alcón, A. W. Cummings, and S. Roche, [Nanoscale Horiz.](#) **9**, 407 (2024).
- [23] Q. H. Wang, K. Kalantar-Zadeh, A. Kis, J. N. Coleman, and M. S. Strano, [Nat. Nanotechnol.](#) **7**, 699 (2012).
- [24] F. Xia, H. Wang, and Y. Jia, [Nat. Commun.](#) **5**, 4458 (2014).
- [25] M. W. Graham, S.-F. Shi, D. C. Ralph, J. Park, and P. L. McEuen, [Nat. Phys.](#) **9**, 103 (2013).
- [26] T. V. Alencar, M. G. Silva, L. M. Malard, and A. M. de Paula, [Nano Lett.](#) **14**, 5621 (2014).
- [27] D. Halbertal, M. Ben Shalom, A. Uri, K. Bagani, A. Y. Meltzer, I. Marcus, Y. Myasoedov, J. Birkbeck, L. S. Levitov, A. K. Geim, *et al.*, [Science](#) **358**, 1303 (2017).
- [28] G. Xing, H. Guo, X. Zhang, T. C. Sum, and C. H. A. Huan, [Opt. Express](#) **18**, 4564 (2010).
- [29] E. Malic, T. Winzer, E. Bobkin, and A. Knorr, [Phys. Rev. B](#) **84**, 205406 (2011).
- [30] T. Winzer, A. Knorr, M. Mittendorff, S. Winnerl, M.-B. Lien, D. Sun, T. B. Norris, M. Helm, and E. Malic, [Appl. Phys. Lett.](#) **101**, 221115 (2012).
- [31] M. Marques and E. Gross, [Ann. Rev. Phys. Chem.](#) **55**, 427 (2004).
- [32] S. Yamada, M. Noda, K. Nobusada, and K. Yabana, [Phys. Rev. B](#) **98**, 245147 (2018).
- [33] Z. Fan, J. H. Garcia, A. W. Cummings, J. E. Barrios-Vargas, M. Panhans, A. Harju, F. Ortman, and S. Roche, [Phys. Rep.](#) **903**, 1 (2021).
- [34] S. M. João, M. Andelković, L. Covaci, T. G. Rappoport, J. M. V. P. Lopes, and A. Ferreira, [R. Soc. Open Sci.](#) **7**, 191809 (2020).
- [35] R. Baer and M. Head-Gordon, [Phys. Rev. Lett.](#) **79**, 3962 (1997).

- [36] R. Baer and M. Head-Gordon, *J. Chem. Phys.* **107**, 10003 (1997).
- [37] P. Ordejón, *Comput. Mater. Sci.* **12**, 157 (1998).
- [38] S. Goedecker, *Rev. Mod. Phys.* **71**, 1085 (1999).
- [39] A. Weiße, G. Wellein, A. Alvermann, and H. Fehske, *Rev. Mod. Phys.* **78**, 275 (2006).
- [40] E. A. A. Pogna, X. Jia, A. Principi, A. Block, L. Banszerus, J. Zhang, X. Liu, T. Sohler, S. Forti, K. Soundarapandian, *et al.*, *ACS Nano* **15**, 11285 (2021).
- [41] D. Brida, A. Tomadin, C. Manzoni, Y. J. Kim, A. Lombardo, S. Milana, R. R. Nair, K. S. Novoselov, A. C. Ferrari, G. Cerullo, and M. Polini, *Nat. Commun.* **4**, 1987 (2013).
- [42] S. Midgley and J. B. Wang, *Phys. Rev. E* **61**, 920 (2000).
- [43] See Supplemental Material at [URL will be inserted by publisher].
- [44] S. Roche, J. Jiang, F. Triozon, and R. Saito, *Phys. Rev. Lett.* **95**, 076803 (2005).
- [45] H. Ishii, S. Roche, N. Kobayashi, and K. Hirose, *Phys. Rev. Lett.* **104**, 116801 (2010).
- [46] L. E. F. Foa Torres, S. Roche, and J.-C. Charlier, *Introduction to Graphene-Based Nanomaterials: From Electronic Structure to Quantum Transport* (Cambridge University Press, 2020).
- [47] V. Dal Lago, E. Suárez Morell, and L. E. F. Foa Torres, *Phys. Rev. B* **96**, 235409 (2017).
- [48] U. Keller, *Ultrafast Lasers* (Springer, 2021).
- [49] J. A. Stratton, *Electromagnetic Theory* (John Wiley & Sons, 2015).
- [50] A. Marini, J. D. Cox, and F. J. García de Abajo, *Phys. Rev. B* **95**, 125408 (2017).
- [51] Y. Yang, G. Kolesov, L. Kocia, and E. J. Heller, *Nano Lett.* **17**, 6077 (2017).